Experiments in Fluids 36 (2004) 246–258
DOI 10.1007/s00348-003-0696-8

Reynolds number effects on a turbulent boundary layer with separation, reattachment, and recovery

S. Song, J.K. Eaton

Abstract The present paper addresses experimental studies of Reynolds number effects on a turbulent boundary layer with separation, reattachment, and recovery. A momentum thickness Reynolds number varies from 1,100 to 20,100 with a wind tunnel enclosed in a pressure vessel by varying the air density and wind tunnel speed. A custom-built, high-resolution laser Doppler anemometer provides fully resolved turbulence measurements over the full Reynolds number range. The experiments show that the mean flow is at most a very weak function of Reynolds number while turbulence quantities strongly depend on Reynolds number. Roller vortices are generated in the separated shear layer caused by the Kelvin–Helmholtz instability. Empirical Reynolds number scalings for the mean velocity and Reynolds stresses are proposed for the upstream boundary layer, the separated region, and the recovery region. The inflectional instability plays a critical role in the scaling in the separated region. The near-wall flow recovers quickly downstream of reattachment even if the outer layer is far from an equilibrium state. As a result, a stress equilibrium layer where a flat-plate boundary layer scaling is valid develops in the recovery region and grows outward moving downstream.

1 Introduction

In most engineering applications, boundary layers are affected by pressure gradient, wall curvature, flow three-dimensionality, wall roughness, or a combination of those perturbations. A boundary layer subject to these perturbations often shows non-equilibrium characteristics. An operable definition for a non-equilibrium boundary layer is a wall shear layer subject to rapid changes in the streamwise direction such that the turbulence cannot be characterized solely in terms of local parameters. A more physical description is that the turbulent eddies at a given streamwise location are not characteristic of the local mean velocity profile. For example, a redeveloping boundary layer downstream of a separation zone has a mean velocity profile resembling a flat-plate boundary layer, but the outer layer contains very energetic eddies associated with the inflectional mean velocity profile in the separated region (Bradshaw and Wong 1972; Song et al. 2000). The boundary layer recovers towards equilibrium by the growth of an internal layer from the wall and the simultaneous decay of the energetic eddies. Conversely, as a boundary layer approaches separation, the mean velocity profile becomes inflectional and the Kelvin–Helmholtz instability can produce large roller vortices. These vortices interact with the existing boundary layer vortices in a way that depends strongly on the parameters of the upstream boundary layer.

These examples of non-equilibrium boundary layer development suggest that the mean flow and turbulence behavior might be sensitive to the flow Reynolds number because the decay rate of non-equilibrium eddies may scale differently with Reynolds number than the growth rate of the internal layer. Although many experiments and numerical simulations have examined simple non-equilibrium boundary layers, information is lacking on Reynolds number effects in these flows.

Recently, two experiments on non-equilibrium boundary layers have been performed using high-resolution laser Doppler anemometers (LDA) and the Reynolds number varied by about an order of magnitude. DeGraaff and Eaton (1999) studied Reynolds number scaling of the turbulent boundary layer on a flat plate and on swept and unswept bumps with the momentum thickness Reynolds number (Re_θ) varying from 1,400 to 24,000. They pointed out that recovering boundary layers from swept and unswept bumps develop a stress equilibrium layer near the wall. The stress equilibrium layer was defined as a wall-adjacent region where the Reynolds stresses are in equilibrium with the local skin friction in a region recovering from perturbations. Ölcmen et al. (2001) investigated Reynolds number effects on two- and three-dimensional turbulent boundary layers outside of a wing/body junction for Re_θ=5,940 and 23,200. In spite of differences in the flow types and conditions, similar trends were observed in the two experiments. The mean flow properties are a weak function of the Reynolds number whereas the turbulence

Received: 11 February 2003 / Accepted: 15 August 2003
Published online: 14 November 2003

S. Song, J.K. Eaton (✉)
Department of Mechanical Engineering,
Stanford University, Bldg 500, Stanford, CA 94305, USA
E-mail: eaton@vk.stanford.edu

Present address: S. Song
Sandia National Laboratories, MS 9951, PO Box 969,
Livermore, CA 94551, USA

We would like to thank the Office of Naval Research for the financial support under grant number N00014-00-1-0078-P00002 supervised by Dr. L. P. Purtell and Dr. R. D. Joslin. Ms. Carolyn Aubertine assisted with PIV data acquisition.

quantities are much more sensitive to the Reynolds number. For example, the normalized Reynolds stress levels increase with the increasing Reynolds number. Unlike flat-plate boundary layers, no known scales collapse all the Reynolds stress profiles for the non-equilibrium flows.

Many important features of separated boundary layers are relatively well understood.The Kelvin–Helmholtz instability produces very energetic eddies that cause inactive motions within the separation zone (Castro and Haque 1987; Adams and Johnston 1988; Simpson et al. 1981b). The details of the eddy development are dependent on the upstream boundary layer characteristics (Eaton and Johnston 1981). In a boundary layer recovering from separation, the turbulence recovers much more slowly than the mean flow, resulting in the turbulence being out of equilibrium with the mean flow field. In addition, the inner part of the boundary layer recovers rapidly developing a stress equilibrium layer (DeGraaff and Eaton 1999) or internal layer (Bradshaw and Wong 1972; Bandyopadhyay and Ahmed 1993; Webster et al. 1996), but the outer part takes a much longer distance to recover. This is because of the persistence of the large eddies carried along from the separated region. In contrast, Alving and Fernholz (1996) and Castro and Epik (1998) suggested that the inner layer would not recover more quickly than the outer layer. This contradiction will be examined in the present paper.

Another open question in separated boundary layer studies is the fate of the large eddies as they pass through the reattachment zone. This is closely related to the rapid reduction in Reynolds stress levels observed in the reattachment zone (Bradshaw and Wong 1972; Eaton and Johnston 1981; Song et al. 2000). An early hypothesis of Bradshaw and Wong (1972) is that the eddies are torn roughly in two near reattachment, reducing their length scale approximately by half. However, many measurements downstream of reattachment show that the large eddies are persisting in the outer layer and that the eddy scale is still comparable to the separation bubble height. Kim et al. (1980) supposed that the eddies move alternatively up and downstream, and Pronchick and Kline (1983) observed that some eddies in a backward-facing step flow are partially swept upstream from reattachment. Another possibility is that the eddies pass roughly unmodified over the top of the reattachment zone as implied in Eaton and Johnston (1981). Driver et al. (1987) showed that the energy spectrum of streamwise velocity fluctuations has the same characteristic frequency up and downstream of reattachment. Bandyopadhyay (1991) argued that the outer layer structure far downstream of reattachment still contains the characteristics of the separated shear layer as far as the turbulent/non-turbulent interface slope is concerned. Hancock (2000) found that the length scale of the outer layer structure downstream of reattachment is reduced by only about 20%.

One possible conclusion that could be extracted from the disparate data interpretations is that the flow structure over the reattachment zone changes little. Some of the large eddies are broken down to smaller scales near reattachment while others remain nearly intact as they pass into the recovery region. The low frequency flapping of the separated shear layer noted by Eaton and Johnston (1981) and Driver et al. (1987), may allow the large eddies to pass through the reattachment zone without severe modifications when the trajectory of the large eddies is far away from the wall. In contrast, the large eddies are probably strongly distorted when the trajectory impinges on the wall at a sharp angle.

Song et al. (2000) presented detailed LDA measurements over the same smoothly contoured ramp as the present experiments for a single Reynolds number, $Re_{\theta,\mathrm{ref}}$=3,500. The mean flow separates approximately three-quarters of the way along the ramp and reattaches a short distance downstream of the ramp trailing edge producing a thin separation bubble. The mean flow recovers quickly downstream of reattachment. As a result, the "law-of-the-wall" is accurate up to y^+=150 at the final measurement station, which is six ramp lengths downstream of the ramp. All the Reynolds stresses increase quickly in the adverse pressure gradient region over the ramp and reach maxima in the reattachment region. The turbulent kinetic energy production has a maximum upstream of separation. The peak in the Reynolds stress profiles is in alignment with the mean profile inflection point in the separated region. The Reynolds stress and turbulent kinetic energy production rate profiles showed that the turbulence is inactive within the separation bubble indicating that the turbulence is caused by the sweeping of the separated shear layer vortices. Downstream of reattachment, the turbulence recovery is slow compared to the mean flow recovery. However, a stress equilibrium layer develops near the wall downstream of reattachment. The Reynolds stress profiles showed that the stress equilibrium layer extends to y^+=70 at the final measurement station although the outer layer still contains energetic large eddies carried from the separated shear layer.

Previous research has made it clear that Reynolds stress production mechanisms are different in separated flows than in flat-plate boundary layers. We should expect that Reynolds number effects on turbulence will also be different. With little information available on these Reynolds number effects, it seems critical to obtain data over a wide range of Reynolds numbers for simple separated flows.

This paper addresses Reynolds number effects in a separating, reattaching, and recovering turbulent boundary layer and provides a benchmark data set for advanced turbulence model development. Even without consideration of the Reynolds number effects, this type of a non-equilibrium boundary layer is challenging to current CFD capabilities because of its highly non-equilibrium nature. The momentum thickness Reynolds number of the upstream boundary layer ranges from 1,100 to 20,100. With the aid of a high-resolution LDA, the near-wall behavior of the flow is examined. Particular emphasis is placed on finding empirical Reynolds number scalings of the mean velocity profiles and the Reynolds stress profiles. This requires identification of length and velocity scales appropriate in the various regions of the flow. Formal dimensional analysis and intuition may lead to successful scaling laws. However, empiricism can provide a useful guide to intuition in complex flows.

2
Experimental apparatus and measurement technique

The experiments were performed in the closed-loop wind tunnel mounted inside a pressure vessel as described by DeGraaff and Eaton (2000). In order to achieve a large range of Reynolds number the vessel pressure is increased up to about 8 atm, and the wind tunnel speed is varied by factor of three while maintaining Mach number less than 0.06. The flow in the wind tunnel is conditioned using a series of honeycombs, screens, and grids followed by a 5:1 two-dimensional contraction. This results in a freestream turbulence intensity of approximately 0.2% at a typical freestream velocity of 15 m/s. The tunnel has a 152 mm high by 711 mm wide development section. The boundary layer is tripped 150 mm downstream of the contraction exit using a rectangular plastic strip 1.6 mm high and 6.4 mm long in the streamwise direction. This allows a development length of about 970 trip heights before the flow is contracted by a special insert that is introduced to form the desired flow geometry as described below.

The spanwise uniformity is examined downstream of reattachment using a single-wire hot wire with 2.5 μm diameter and 600 μm active length. The hot-wire probe is a custom-made, boundary layer probe described by Littell and Eaton (1994). The flow is measured at four spanwise locations at each of five different streamwise locations. In addition, total pressure is measured near the buffer layer in the recovery region. The results are omitted here for brevity. They show a high degree of spanwise uniformity.

Figure 1 shows the flow geometry. The flow in the development section mildly contracts over a length of 69 mm on the bottom wall. The contraction is defined by a 5th order polynomial and reduces the tunnel height from 152 mm to 131 mm. The boundary layer relaxes to its equilibrium characteristics on a 320 mm long flat plate, then passes over a smoothly contoured ramp, and a 630 mm long downstream flat plate followed by a diffuser. The ramp is a circular arc with a 127 mm radius. The ramp height (h) and length (L) are 21 mm and 70 mm, respectively. The inlet of the flow is defined on the 320 mm flat plate, two ramp lengths (140 mm) upstream of the ramp beginning. The boundary layer separates about three-quarters of the way along the ramp and reattaches on the downstream flat plate, a short distance downstream of the ramp trailing edge. As a consequence, a separation bubble is generated centered around the trailing edge. The points of separation and reattachment were determined by scanning the streamwise velocity 60 μm above the surface with 0.5 mm spacing in the streamwise direction. The points with zero velocity were defined as the separation and reattachment points. The downstream flat plate is about nine ramp lengths (630 mm) long, allowing the flow to recover from the perturbation.

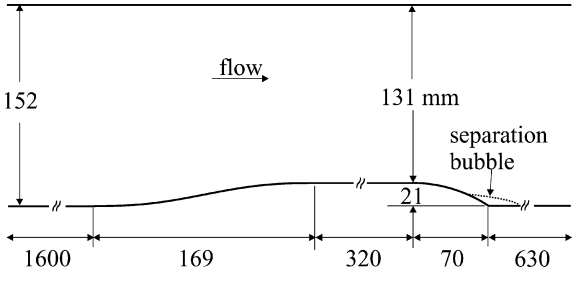

Fig. 1. Flow geometry

In order to accurately measure turbulence quantities at high Reynolds numbers, a high-resolution measurement technique is necessary. We used a custom, two-component, high-resolution LDA with a measurement volume of 35 μm in diameter by 60 μm in length described in DeGraaff and Eaton (2001). This LDA uses a series of beam conditioning optics and side scattering collection optics to achieve the small measurement volume. LDA biases including fringe bias, validation bias, velocity bias, and velocity gradient bias are either avoided or corrected as suggested in DeGraaff and Eaton (2001). Typical uncertainties in U, $\overline{u'^2}$, $\overline{v'^2}$, and $\overline{u'v'}$ are given in Table 1 for the LDA measurements, where 5,000 samples at each data point were collected. The uncertainty estimate is based on various uncertainty sources: statistical uncertainty, data filtering, fringe spacing estimation, velocity bias correction, etc.

Two-dimensional, digital PIV measurements were performed to provide information on instantaneous spatial structure and two-point correlations to be presented in another paper. For the purposes of the present paper, however, PIV measurements serve to corroborate the LDA measurements. Figure 2a, b shows LDA and PIV measurements of U and $-\overline{u'v'}$ at reattachment for an inlet momentum thickness Reynolds number of 3,400. The agreement is very good in all the profiles despite the difficult experimental conditions. Note that the turbulence intensity reaches a maximum and that the mean velocity gradient is very high in the reattachment zone. Figure 2b includes uncertainty bars only for PIV measurements for clarity. For the mean velocity profile, the uncertainty bars for both PIV and LDA measurements are smaller than the symbol size, and they are omitted. The agreement between the LDA and PIV data for $\overline{u'^2}$ and $\overline{v'^2}$ is as good as for $-\overline{u'v'}$ although they are not shown here. Similar agreement between LDA and PIV measurements was obtained throughout the measurement domain.

More detailed information on the experimental facilities and measurement techniques can be found in Song and Eaton (2002b).

3
Reynolds number effects on mean velocity and Reynolds stress profiles

The flow was measured at five different Reynolds numbers. The momentum thickness Reynolds numbers evaluated at a reference station, $Re_{\theta,\mathrm{ref}}$, are 1,100, 3,400, 7,100, 13,200,

Table 1. LDA and PIV uncertainty guidelines. The percentage value are based on local values of measurements

	LDA	PIV
U	±1.5%	±0.5%
$\overline{u'^2}$	±4%	±7%
$\overline{v'^2}$	±8%	±7%
$\overline{u'v'}$	±10%	±10%

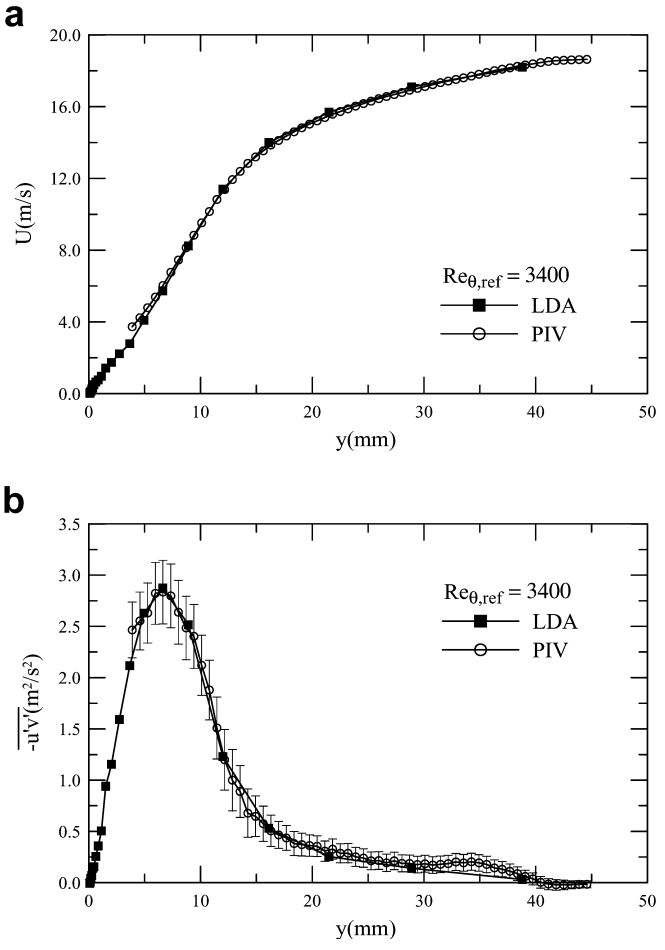

Fig. 2. a Streamwise mean velocity at reattachment.; **b** Reynolds shear stress at reattachment

and 20,100. The coordinate system adapted herein is such that x' indicates the streamwise distance normalized by the ramp length (70 mm). The y coordinate is maintained normal to the flat plate in the test section. The beginning of the ramp is set to x'=0.00 and the trailing edge x'=1.00. The reference station is defined at x'=−2.00. Table 2 shows flow conditions for each case.

3.1 Overall Reynolds number effects on the flow development

Figure 3 shows the streamwise mean velocity development for two Reynolds numbers, $Re_{\theta,ref}$=3,400 and 20,100. As the flow passes over the ramp, the boundary layer thickens rapidly and then separates three-quarters of the way along the ramp and reattaches approximately a third of the ramp length downstream of the ramp trailing edge. The mean separation and reattachment points are at most a very weak function of Reynolds number as shown in Table 3. However, this is not true for the lowest Reynolds number case where the separation bubble is considerably longer, indicating that extrapolation of the low Reynolds number results may lead to inaccurate prediction for high Reynolds number separated flow applications. This is consistent with recent results from DeGraaff and Eaton (2000) showing that a flat-plate boundary layer at Re_θ=1,430 has

Table 2. Flow conditions

$Re_{\theta,ref}$	$U_{e,ref}$ (m/s)	δ_{99} (mm)	Temp (K)	Pressure (Pa)	$\nu\times10^6$ (m^2/s)
1,100	6.52	25.6	293.0	101,300	15.1
3,400	20.2	27.6	297.0	101,300	15.5
7,100	11.0	29.0	300.0	456,000	3.92
13,200	20.3	26.5	301.5	473,000	3.40
20,100	20.5	26.0	301.5	782,000	2.06

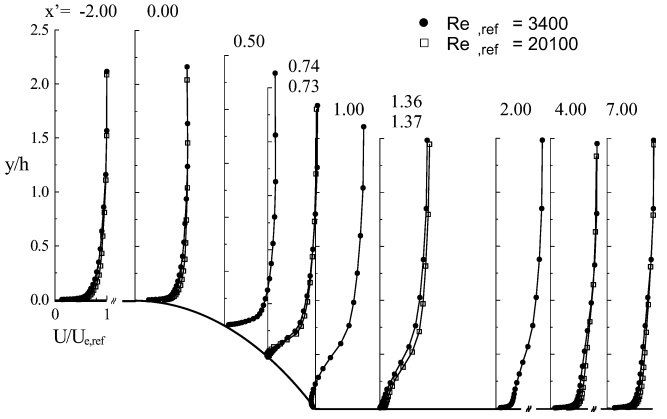

Fig. 3. Overall Reynolds number effect on mean flow development. Vertical scale is expanded

Table 3. Mean separation and reattachment locations

$Re_{\theta,ref}$	Separation (x')	Reattachment (x')
1,100	0.40	1.36
3,400	0.74	1.36
7,100	0.74	1.40
13,200	0.76	1.39
20,100	0.73	1.37

different Reynolds stress behavior than higher Reynolds number boundary layers. Because of this anomalous flow behavior, the lowest Reynolds number case will be excluded or ignored in most discussion hereafter.

The weak dependence of the mean separation point on Reynolds number is a clear indication that the momentum transport, the mean stress gradients, and the Reynolds stress gradients scale the same way in the neighborhood of separation. The mean momentum transport and stress gradients scale with ρU_e^2, and it will be shown below that the Reynolds shear stress has the same scaling near separation. There is unpublished anecdotal evidence of Reynolds number effects on separation location, but those observations may be related to roughness effects (Song and Eaton 2002a).

Figure 4 shows the overall Reynolds number effects on the development of the streamwise Reynolds normal stress component for the two Reynolds numbers. The stress is normalized using the mixed scaling suggested in DeGraaff and Eaton (2000) for flat-plate boundary layers. Unlike the mean profiles, Reynolds number effects are strong, especially in the separated region where the stresses are much

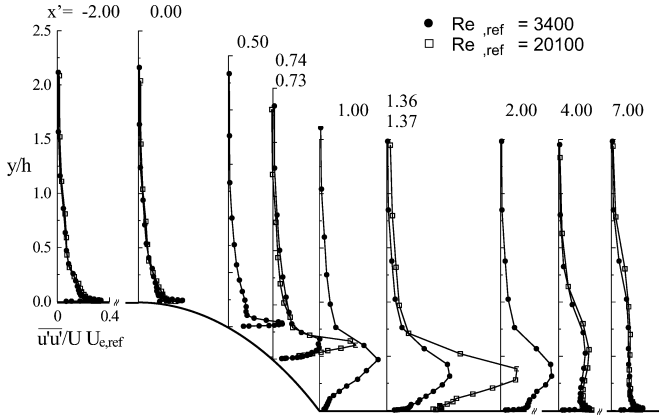

Fig. 4. Overall Reynolds number effect on $\overline{u'^2}$ development. The stress is normalized by $U_\tau U_{e,ref}$ of the individual Reynolds number

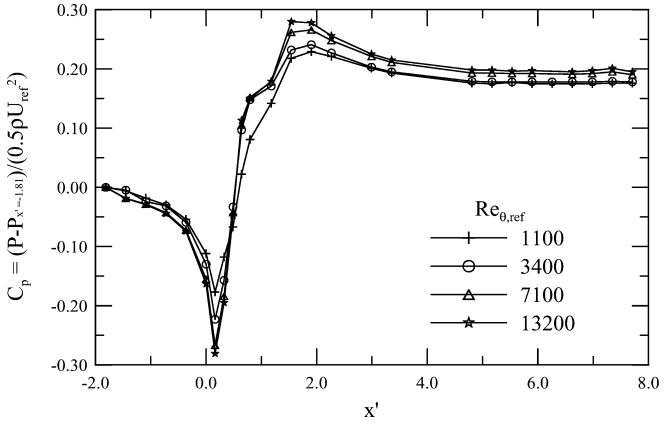

Fig. 5. Wall-static pressure distribution on the bottom wall

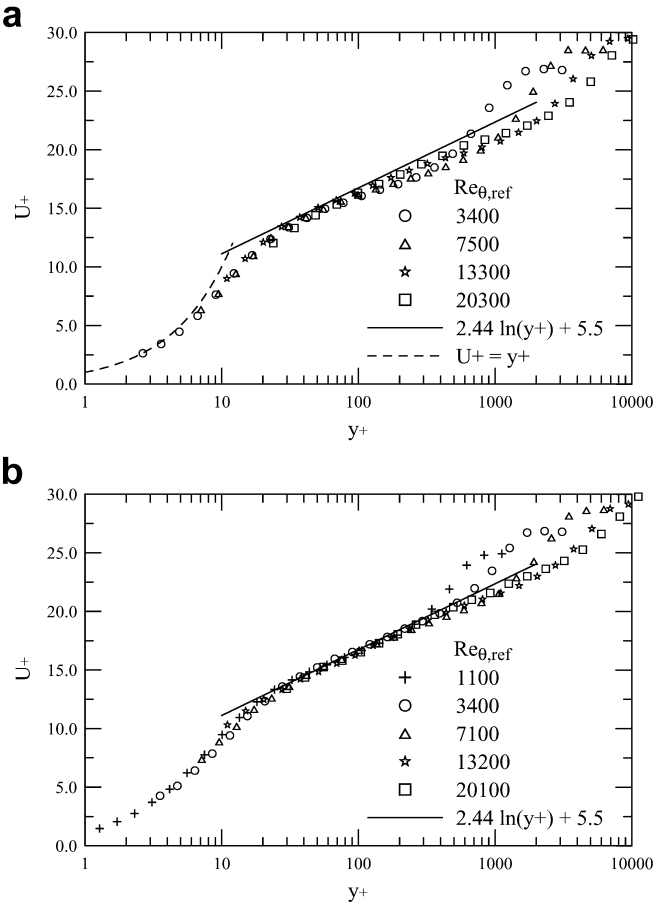

Fig. 6a, b. The "law-of-the-wall" plots in the recovery region. a x'=4.00; b x'=7.00

larger for the higher Reynolds number case. The other measured stress components are not shown here for brevity, but the overall Reynolds number effects are similar.

3.2
Reynolds number effects on the mean flow

Figure 5 shows the wall-static pressure (C_p) distributions for four Reynolds numbers. The pressure distribution on the tunnel floor does not depend on Reynolds number over the ramp, but it does downstream of the ramp trailing edge. The Reynolds number effects are most evident in the reattachment zone where the pressure recovery increases with increasing Reynolds number. Note that there is a short distance over the ramp subject to a favorable pressure gradient caused by the ramp curvature. The recovery region also shows weak Reynolds number effects. The pressure distribution on the tunnel top wall (not shown) varies smoothly and indicates that there is no counter separation on the top wall.

Mean velocity "law-of-the-wall" plots for the recovery region are shown in Fig. 6a, b. The skin friction was measured using the oil-flow interferometry technique (Monson et al. 1993) except for the $Re_{\theta,ref}$=1,100 case. Uncertainty of the measurements was estimated to ±4%. For $Re_{\theta,ref}$=1,100, a conventional log-law fitting was used because the flow required an oil with a too low viscosity. Multiple mean velocity measurements are available in the sublayer at this Reynolds number, so the skin friction can be inferred accurately from the mean profile. Figure 6a, b shows that the logarithmic layer has not been reestablished by x'=4.00 for any Reynolds number, but that a well developed logarithmic region extends out to about y^+=200 at x'=7.00. Both sets of profiles show the characteristic dip below the logarithmic line commonly found in recovering boundary layers. These data provide the first indication that a stress equilibrium layer is developing in the recovery region. The Reynolds stress data described below provide further verification.

The Reynolds number effects on the mean flow in the recirculation region can be examined by looking at scalar parameters describing the backflow velocity profile. Table 4 shows the separation bubble thickness, the peak backflow velocity, and the height of the peak backflow velocity all measured at the ramp trailing edge. The maximum backflow velocity (U_N) scales on the local freestream velocity except for the lowest Reynolds number. It is interesting to note that the maximum backflow velocity is considerably lower ($0.086U_e$) than $0.2U_e$ commonly found in backward-facing step flows (Adams and Johnston 1988). For the present relatively thin separation bubble, separated shear layer structures reach all the way to the wall producing only intermittent backflow (Simpson et al. 1981b). Neither the measured separation bubble

Table 4. Backflow parameters at x'=1.00. Re_h: the ramp height Reynolds number using $U_{e,ref}$,S: the separation bubble height, N: the height at $U=-U_N$

$Re_{\theta,ref}$	Re_θ	Re_h	S (mm)	N (mm)	U_N (m/s)	$\sqrt{U_N N/\nu}$	U_N/U_e
1,100	1,800	9,100	5.5	1.8	0.71	9.20	0.12
3,400	5,600	27,400	4.3	1.4	1.63	12.1	0.086
7,100	11,100	58,900	5.4	1.8	0.90	20.3	0.087
13,200	21,800	125,000	5.0	1.3	1.67	25.3	0.087

Table 5. Inflection point height (y_{infln}, mm) and velocity (U_{infln}, m/s)

	Separation		Trailing edge		Reattachment	
$Re_{\theta,ref}$	y_{infln}	U_{infln}	y_{infln}	U_{infln}	y_{infln}	U_{infln}
3,400	3.5	6.9	10.8	7.2	8.2	7.6
7,100	4.1	4.8	11.3	4.2	9.2	4.5
13,200	4.1	9.9	10.7	8.2	8.5	8.9
20,100	3.9	11.3	N/A	N/A	9.0	9.4

height (S) nor the height of the maximum backflow velocity (N) varied monotonically with Reynolds number. It is clear though that the Reynolds number scaling of the maximum backflow height does not follow the scaling proposed by Adams and Johnston (1988). Table 5 shows the height of the inflection point in the mean velocity profile at three streamwise positions in the separation region. There is some variability indicating the uncertainty in locating the inflection point. However, within uncertainty the inflection point height seems to be nearly constant with varying Reynolds number. This further backs up the assertion that the mean flow is very weakly affected by the Reynolds number.

Figure 7a shows velocity deficit profiles at the reference station using the Zagarola and Smits (1998) scaling ($U_e\delta^*/\delta_{99}$). The profiles are in good agreement down to y/δ_{99}=0.2. Figure 7b shows that the same scaling also works well at x'=0.00, which is subject to favorable pressure gradient. Note that the scaled profiles at x'=0.00 are in reasonably good agreement with the reference profile. Since the outer layer responds more slowly to a pressure gradient than the inner layer (Smits and Wood 1985), the agreement with the reference profile indicates that the effects of the favorable pressure gradient have not penetrated the outer boundary layer yet. Castillo and George (2001) argued that this scaling ($U_e\delta^*/\delta_{99}$) is universal for favorable pressure gradients, but their assumption that Reynolds shear stress scales on the outer variables is questionable. More detailed studies for various favorable pressure gradients and a large range of Reynolds number are required to be conclusive.

Figure 8 shows the velocity deficit profiles at separation. Note that separation occurred earlier (x'=0.40) for $Re_{\theta,ref}$=1,100. The deficit profiles collapse reasonably well at separation, but they do not coincide with the flat-plate profile.

For the recovery region, the $U_e\delta^*/\delta_{99}$ scaling is again robust. Figure 9a, b shows the deficit profiles at x'=4.00 and 7.00. The x'=4.00 profiles are not in very good agreement but the x'=7.00 profiles show excellent agreement for the outer 95% of boundary layer, approximately. The DeGraaff and Eaton (2000) data for a flat-plate boundary layer at Re_θ=5,200 are included in Fig. 9b. The difference between the recovery region and the flat-plate profiles is small but significant considering the excellent agreement between the local profiles.

3.3 Reynolds number effects on the Reynolds stresses

A characteristic of non-equilibrium boundary layers is that the different Reynolds stress components evolve at different rates. This makes the scaling behavior very complicated. We have found empirical scaling laws for each of the three measured stress components in each

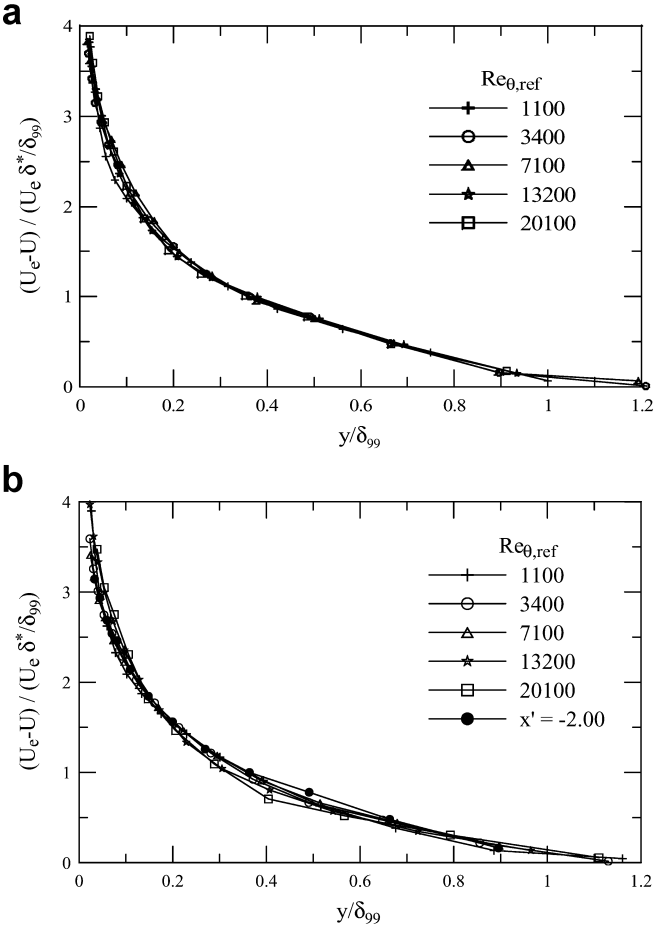

Fig. 7a, b. Velocity deficit scaling using $U_e\delta^*/\delta_{99}$. **a** x'=−2.00; **b** x'=0.00

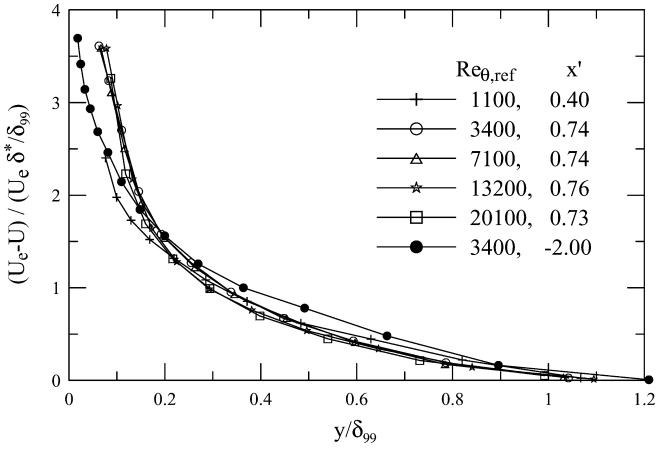

Fig. 8. Velocity deficit scaling using $U_e\delta^*/\delta_{99}$ at separation

region of the flow. While these empirical scalings are probably not unique and may only apply to this particular flow, they do help understand both the physics and potentially the modeling of the various regions of the flow. Also, it is likely that similar scalings apply to other separated and reattaching flows. The empirical scalings are summarized in Table 6 and the data collapse for various stress components is described below.

At the reference station, the flat-plate boundary layer scaling suggested by DeGraaff and Eaton (2000) is valid for both inner and outer layers, although the profiles are not shown here for brevity. The profiles of $-\overline{u'v'}$ are a little scattered because of the higher uncertainty in this component, but are still in reasonably good agreement.

The Reynolds stresses at x'=0.00 already show some deviation from flat-plate behavior because of the favorable pressure gradient. The mixed scaling for $\overline{u'^2}$ fails at x'=0.00 as the peak level of $\overline{u'^2}/U_\tau U_e$ increases with increasing Reynolds number. We found that the $\overline{u'^2}$ profiles collapse better in the outer variable scaling $\left(\overline{u'^2}/U_e^2\right)$ except for $Re_{\theta,\mathrm{ref}}$=1,100 as shown in Fig. 10a. The wall shear stress is high at this location because of the flow acceleration, so the peak in $\overline{u'^2}$ occurs too close to the wall to measure accurately at the two highest Reynolds numbers. The peak levels of normalized $\overline{v'^2}$ and $-\overline{u'v'}$ shown in Fig. 10b, c are lower than the reference boundary layer because of the rapid increase in wall shear stress. Interestingly, the profiles still collapse well in inner scaling. This confirms that $\overline{v'^2}$ and $-\overline{u'v'}$ behave similarly to each other for

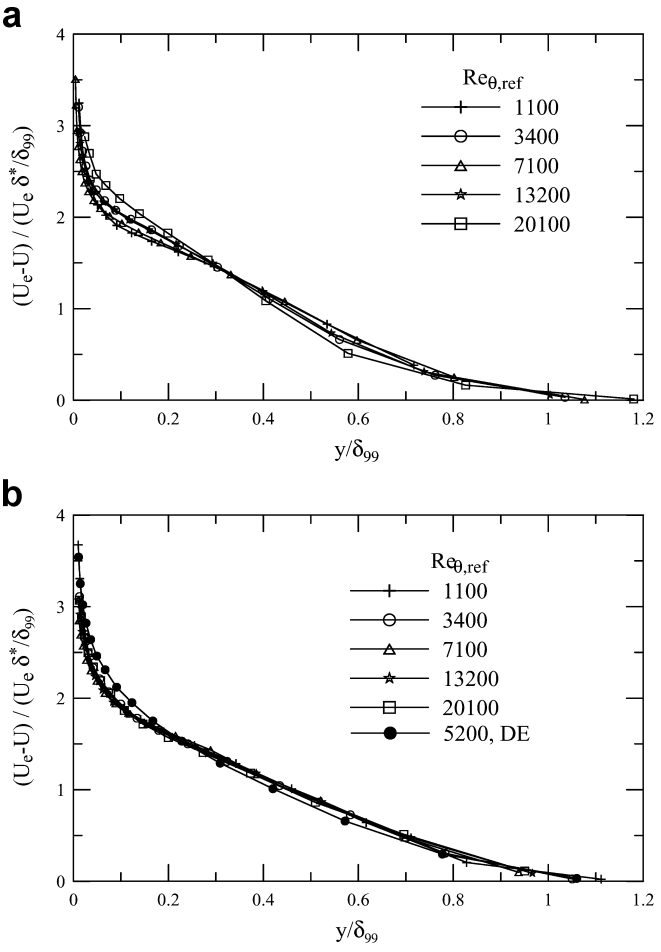

Fig. 9a, b. Velocity deficit scaling using $U_e\delta^*/\delta_{99}$. **a** x'=4.00; **b** x'=7.00. *DE* denotes DeGraaff and Eaton (2000)

non-equilibrium boundary layers since both of them are influenced by the active motions.

As suggested in Fig. 4, Reynolds number scaling in the separated region is expected to be much different from the flat-plate boundary layer scaling because Kelvin–Helmholtz roller vortices are generated in the separated shear layer. The mean profile contains an inflection point where the turbulent kinetic energy production rate is maximum as described in Song et al. (2000). Profiles plotted using empirically derived scalings are presented in Figs. 11, 12, and 13 with the vertical height normalized by the inflection

Table 6. Reynolds number scaling for Reynolds stress. S.E.L. denotes stress equilibrium layer

Reynolds stress	x'=−2.00		x'=0.00
$\overline{u'^2}$	$U_\tau U_e$		U_e^2
$\overline{v'^2}$	U_τ^2		U_τ^2
$-\overline{u'v'}$	U_τ^2		U_τ^2
Reynolds stress	Separation	Trailing edge	Reattachment
$\overline{u'^2}$	$U^2_{\mathrm{inf\,ln,reatt}}$	$U^2_{\mathrm{inf\,ln}}$	$U^2_{\mathrm{inf\,ln}}$
$\overline{v'^2}$	$U^2_{\tau,\mathrm{ref}}$	$U^2_{\mathrm{inf\,ln}}$	$U^2_{\mathrm{inf\,ln}}$
$-\overline{u'v'}$	U_e^2	$U^2_{\mathrm{inf\,ln}}$	$U^2_{\mathrm{inf\,ln}}$
Reynolds stress	S.E.L.		Outer layer in recovery region
	$U_\tau U_e$		$U_\tau U_e$
	U_τ^2		U_e^2
	U_τ^2		U_τ^2

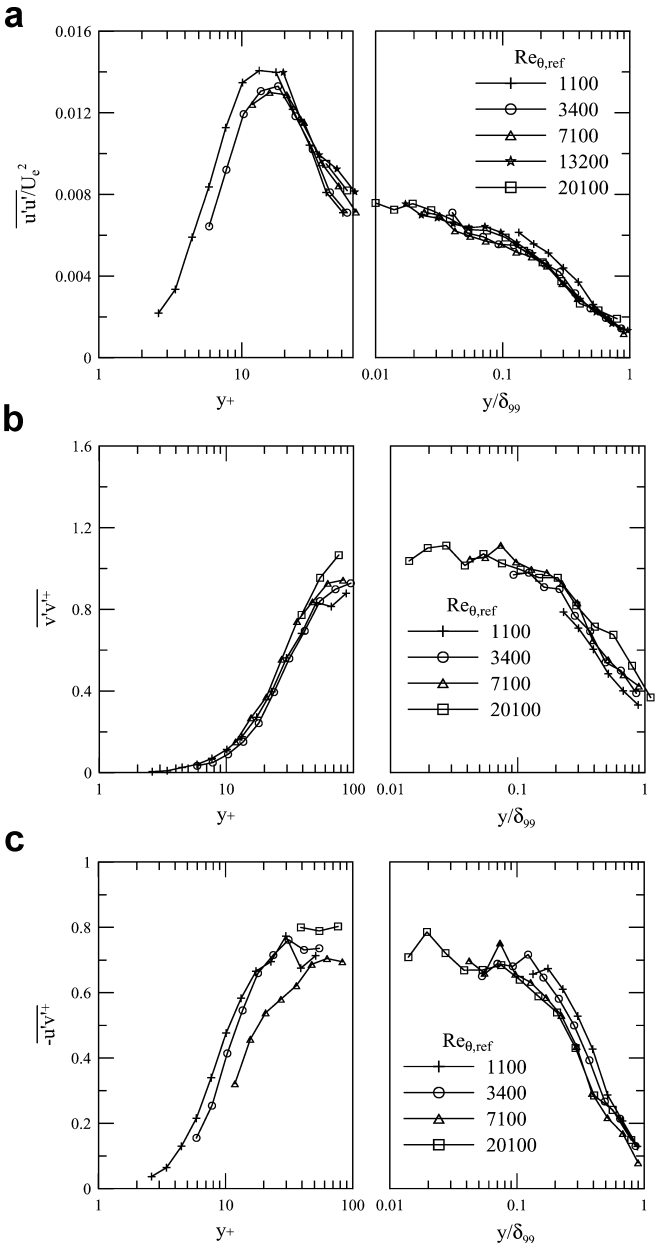

Fig. 10a–c. Reynolds number scaling for Reynolds stresses at x'=0.00. **a** $\overline{u'^2}$; **b** $\overline{v'^2}$; **c** $-\overline{u'v'}$

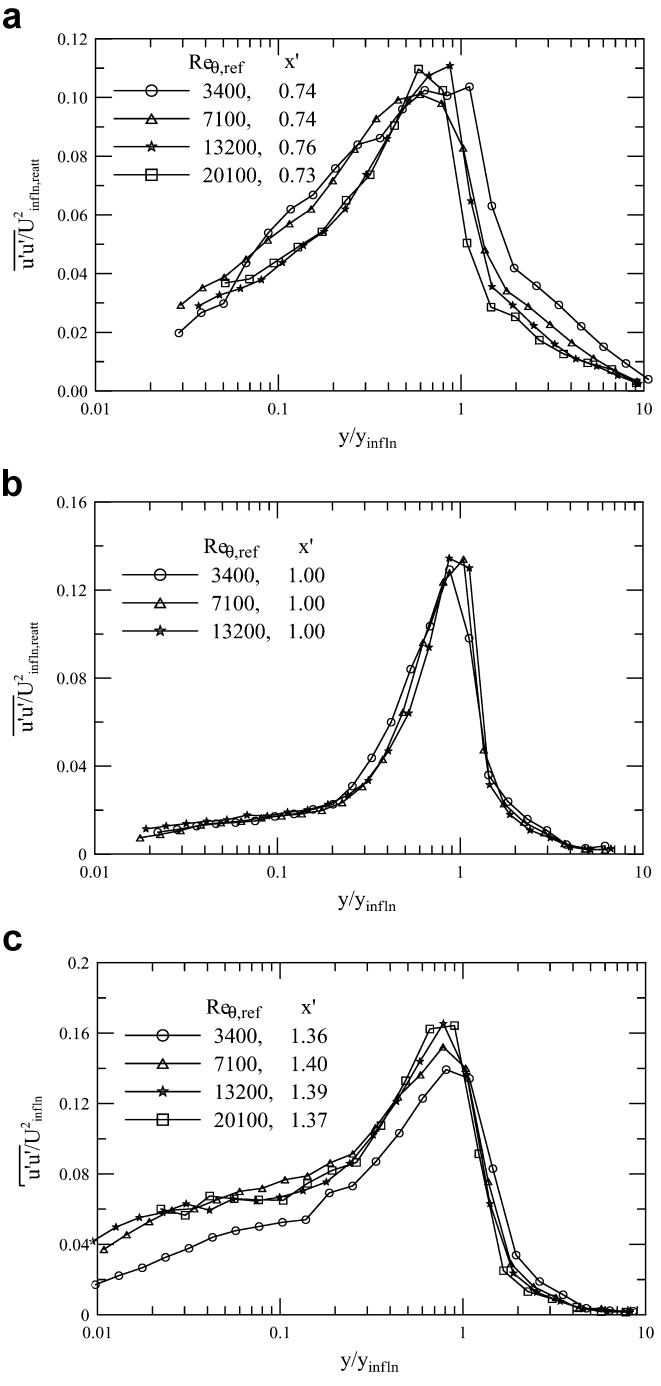

Fig. 11. Reynolds number scaling for $\overline{u'^2}$ in the separated region: **a** at separation; **b** x'=1.00; **c** at reattachment

point height in the corresponding mean velocity profile. Table 5 shows inflection point heights ($y_{\text{in fln}}$) and the mean velocities ($U_{\text{in fln}}$) at the inflection point in the separated region. Note that Table 5 shows that there are actually subtle changes to the mean velocity profile between cases. The ratio of the inflection point velocity to the freestream velocity increases monotonically from 0.38 to 0.46 as the Reynolds number increases from 3,400 to 20,100.

The streamwise Reynolds normal stress, $\overline{u'^2}$, scales on a fixed velocity for all the three streamwise locations (separation, trailing edge, and reattachment) as shown in Fig. 11a–c. We chose to use the inflection point mean velocity evaluated at reattachment ($U_{\text{inf ln,reatt}}$), but $U_{\text{inf ln}}$ measured at the ramp trailing edge collapses the data almost as well. The plots show that the stress peaks collapse fairly well in the inflection point scaling and the overall agreement of the entire profile is quite good. This indicates that the high levels of $\overline{u'^2}$ in the separated zone are mainly produced by large-scale, low frequency motions of the separated shear layer (Eaton and Johnston 1981; Driver et al. 1987). Alving and Fernholz (1996) suggested that the shear layer oscillates as "lumps" of the fluid are exchanged between the shear layer and the reverse-flow region. An appropriate scale for the streamwise velocity fluctuations produced in this way is the mean velocity difference across the shear layer. This is well represented by the inflection point mean velocity.

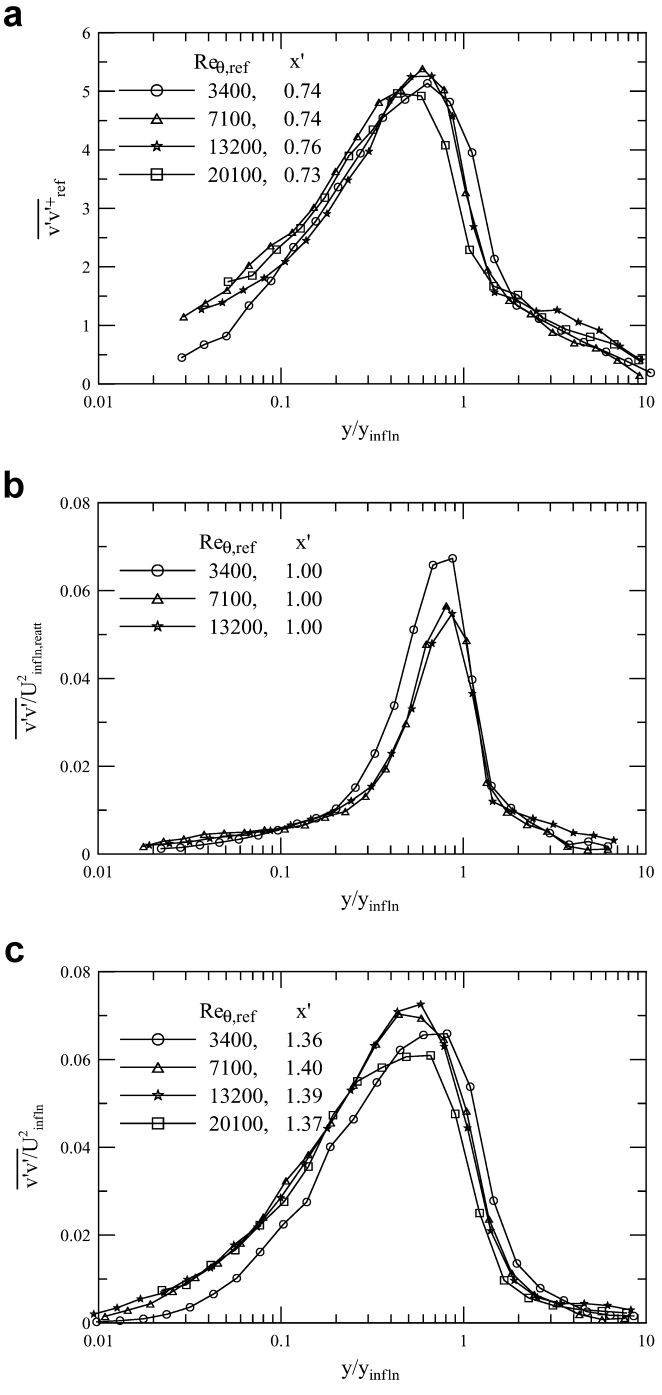

Fig. 12. Reynolds number scaling for $\overline{v'^2}$ in the separated region: **a** at separation; **b** x'=1.00;**c** at reattachment

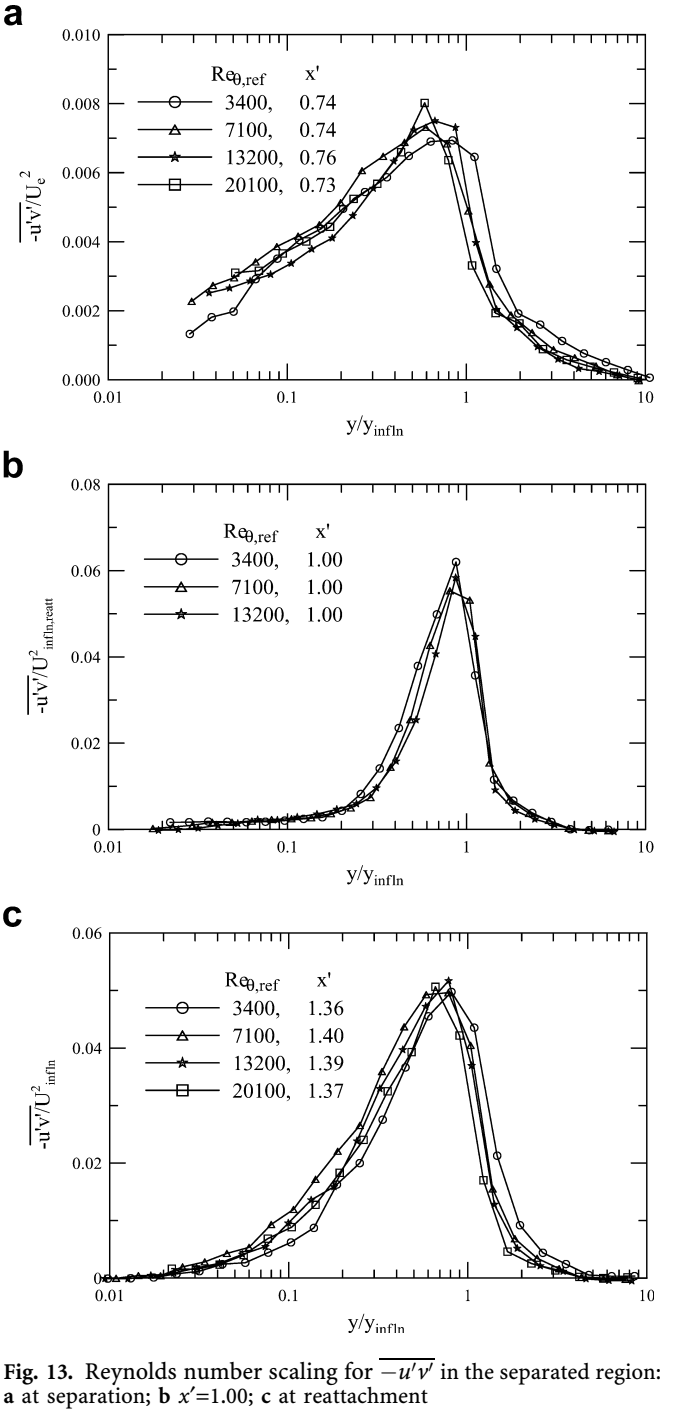

Fig. 13. Reynolds number scaling for $-\overline{u'v'}$ in the separated region: **a** at separation; **b** x'=1.00; **c** at reattachment

The $\overline{v'^2}$ profiles at separation scale on the friction velocity evaluated at the reference station whereas the inflection point scaling holds at the trailing edge and reattachment. The scaled $\overline{v'^2}$ profiles in the separated region are shown in Fig. 12a–c. The collapse is good in general. The trailing edge profile for $Re_{\theta,\mathrm{ref}}$=3,400 is higher than the others, but the differences are not large considering the uncertainty. Given that the active motions contribute to $\overline{v'^2}$ and $U_{\tau\tau}$ in a flat-plate boundary layer, it seems that the upstream active motions dominate $\overline{v'^2}$ all the way to separation. However, the separated shear layer eddies that scale on the velocity difference across the shear layer dominate $\overline{v'^2}$ in the separated region.

The profiles of $-\overline{u'v'}$ at separation collapse using the outer scaling (U_e) as shown in Fig. 13a. However, the $-\overline{u'v'}$ profiles collapse using the inflection point scaling at the trailing edge and reattachment as shown in Fig. 13b, c. When the outer variable scaling (U_e and δ_{99}) was applied in the separated region, the collapse of the profiles was again poor. For example, the peak $\overline{u'v'}/U_e^2$ at reattachment is 52% higher for $Re_{\theta,\mathrm{ref}}$=20,100 than for $Re_{\theta,\mathrm{ref}}$=3,400 (Song and Eaton 2002b).

The inflection point scaling used in the separation region physically makes sense because the maximum

turbulent kinetic energy production rate occurs at the inflection point. The height of peak stress is well aligned with the inflection point height for the entire separated region. All the stress profiles at the trailing edge and reattachment collapse using inflection point scaling. The inflection point scaling is similar to plane mixing layer scaling that uses the average of the upper- and lower-layer velocities.

The inflection point scaling should not be confused with the Perry and Schofield (1973) scaling that is valid in adverse pressure gradient regions (Samuel and Joubert 1974; Simpson et al. 1981a; Schofield 1981). The two scalings are similar in that they use the information at or near the point of maximum shear stress. However, the Perry and Schofield (1973) scaling deduces two velocity scales from the maximum shear stress and their half-law fitting. Also, this scaling is limited to the region upstream of separation since it uses U_τ, which is zero at separation and reattachment. The inflection point scaling is valid in the separated region.

Interestingly, it was found that the outer scaling (U_e) also holds for $\overline{v'^2}$ and $\overline{u'v'}$ at the trailing edge (x'=1.00) although the profiles are not shown for brevity. The collapse is as good as in Figs.12b and 13b. However, the $\overline{u'^2}$ profiles do not collapse using the outer scaling. This might be because $\overline{u'^2}$ in the separated region is affected by the low frequency flapping of the separated shear layer. The fact that $\overline{v'^2}$ and $-\overline{u'v'}$ collapse in outer scaling implies that large-scale vortices grow in the separated shear layer similar to plane mixing layers.

The suggested scalings over the ramp would not change significantly if a ramp surface-normal coordinate was used or equivalently if a flat-plate boundary layer was forced to separate and reattach with an appropriate streamwise pressure gradient. It is well known that a convex wall curvature reduces outer layer turbulence (Gillis and Johnston 1983). In the present experiments, however, the pressure gradient effects were strong enough to overwhelm any possible effects of the wall curvature. Thus, unless a strange boundary condition such as blowing or suction was applied, the appropriate pressure gradient to a flat-plate boundary layer would result in the same Reynolds stress scalings.

In the recovery region, the flat-plate boundary layer scaling of DeGraaff and Eaton (2000) is valid near the wall where a stress equilibrium layer is developing for the full range of Reynolds number. Figures 14, 15, and 16 show the Reynolds stress profiles for the three stress components in the stress equilibrium layer. The plots at x'=7.00 include a flat-plate profile taken from DeGraaff and Eaton (2000) for comparison. The flat-plate boundary layer scaling collapses the three stress components reasonably well up to y^+=40 or 50 at x'=4.00 and up to y^+=70 at x'=7.00. This is consistent with the validity of the law of the wall in the recovery region. These plots also show that the flat-plate

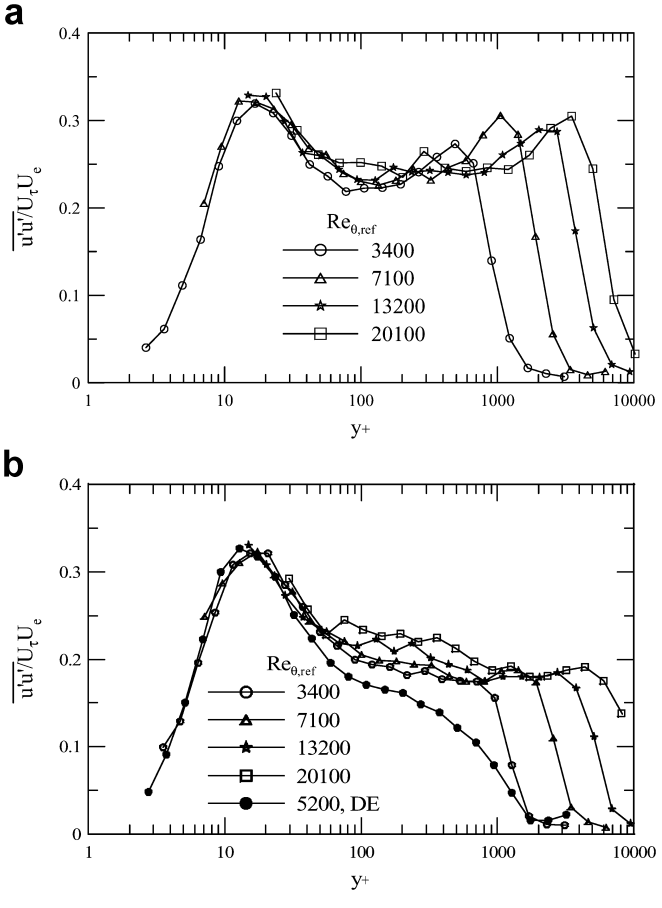

Fig. 14a–b. Reynolds number scaling for $\overline{u'^2}$ in the stress equilibrium layer. **a** x'=4.00; **b** x'=7.00. *DE* denotes DeGraaff and Eaton (2000)

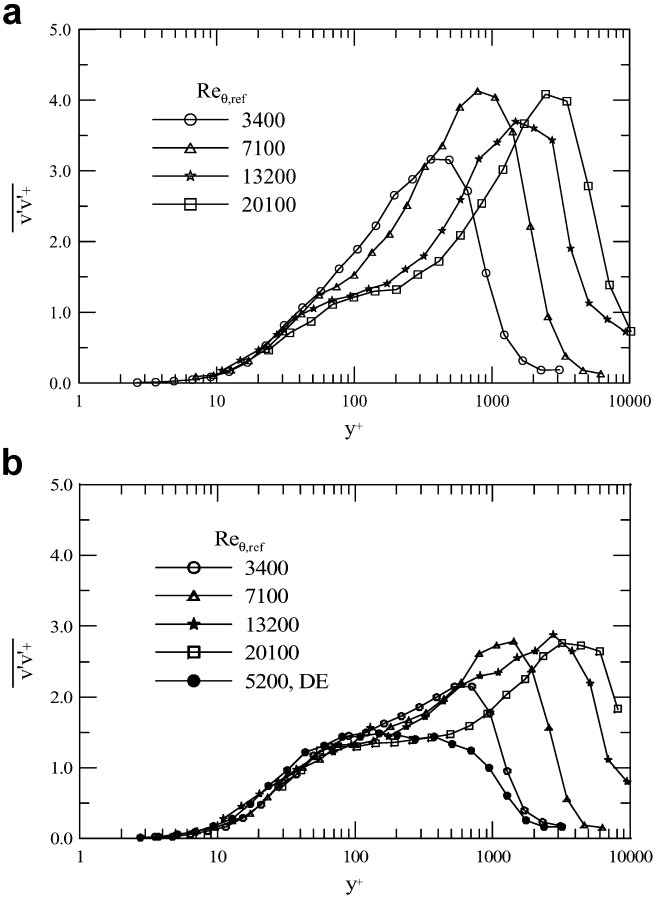

Fig. 15a, b. Reynolds number scaling for $\overline{v'^2}$ in the stress equilibrium layer. **a** x'=4.00; **b** x'=7.00. *DE* denotes DeGraaff and Eaton (2000)

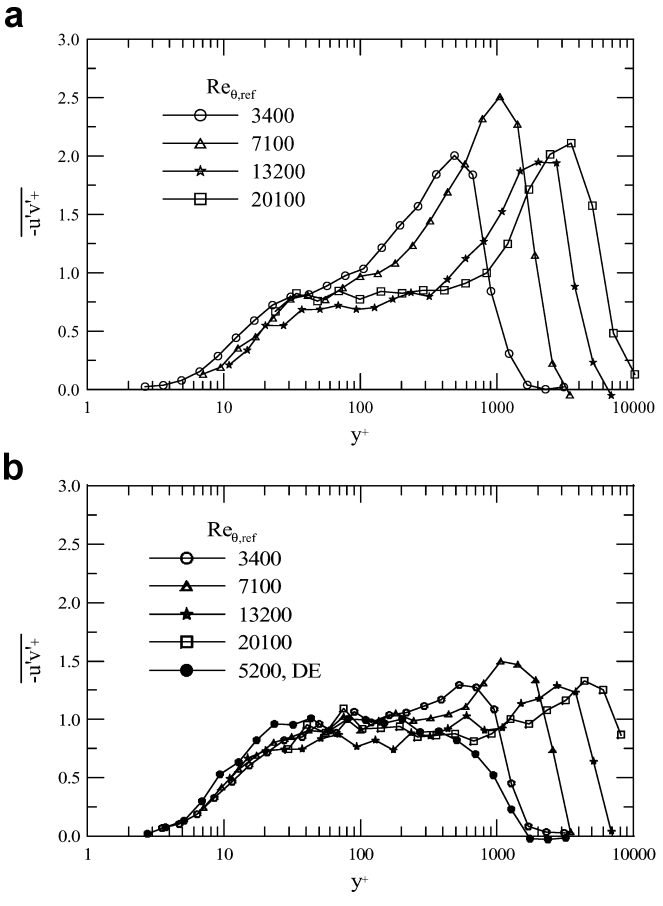

Fig. 16a, b. Reynolds number scaling for $-\overline{u'v'}$ in the stress equilibrium layer. **a** x'=4.00; **b** x'=7.00. *DE* denotes DeGraaff and Eaton (2000)

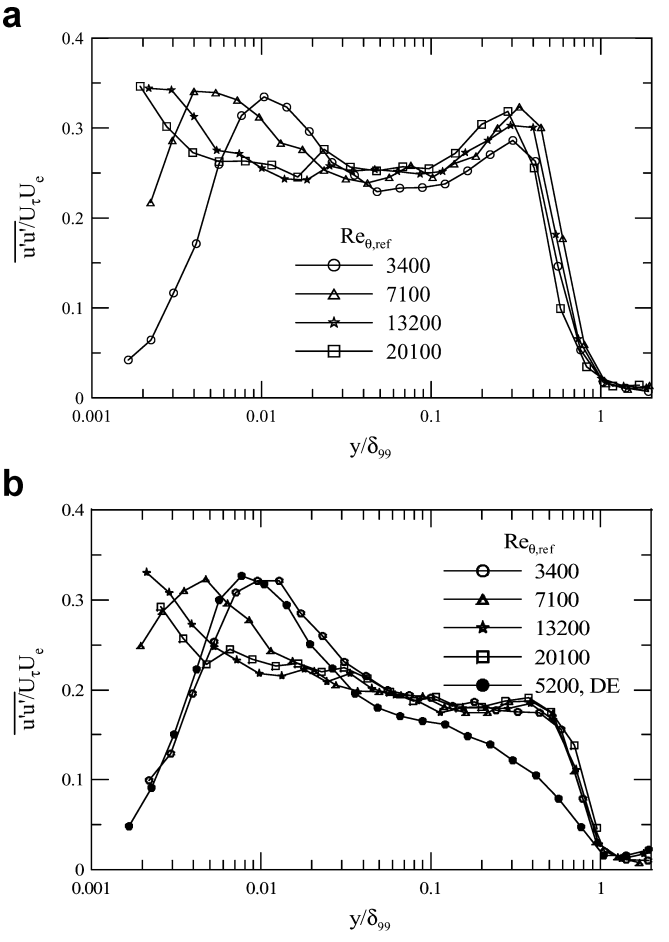

Fig. 17a, b. Reynolds number scaling for $\overline{u'^2}$ for the outer layer in the recovery region. **a** x'=4.00; **b** x'=7.00. *DE* denotes DeGraaff and Eaton (2000)

scaling fails in the outer layer of the non-equilibrium boundary layer.

DeGraaff and Eaton (1999) also reported that a stress equilibrium layer develops downstream of a mild adverse pressure gradient region without separation. Thus, the development of the stress equilibrium layer seems independent of the details of the upstream flow disturbance. Castro and Epik (1998) have stated that a stress equilibrium layer (or internal layer) would not develop in the recovering boundary layer downstream of a large separation bubble where the size of the separated zone is much larger than the upstream boundary layer. However, the present case causes a strong perturbation throughout the boundary layer compared to the DeGraaff and Eaton (1999) perturbations, yet the stress equilibrium layer develops quickly. Further measurements with high-resolution measurement techniques very near the wall in more strongly perturbed flows are required to reach a firm conclusion.

The fact that the flat-plate boundary layer scaling holds in the stress equilibrium layer for high Reynolds number flows suggests that a simple wall model can be applied to the stress equilibrium layer for CFD to avoid excessive grid requirements near the boundary. Factors controlling the development rate of the stress equilibrium layer are not known. The rate must be strongly related to streamwise pressure gradient. The shear stress gradient at the wall is determined by the pressure gradient. It is unlikely that a stress equilibrium layer can develop if the pressure gradient is changing rapidly. The development rate might depend on the strength of perturbation. However, it is evident that the stress equilibrium layer exists near the wall downstream of perturbations regardless of Reynolds number.

In the outer layer of the recovery region, each Reynolds stress component decays at a different rate, so the flat-plate boundary layer scaling does not hold. While the $\overline{u'^2}$ profiles collapse reasonably well in the mixed scaling as shown in Fig. 17a, b, the $\overline{v'^2}$ profiles are scaled by the outer scaling, U_e, as shown in Fig. 18a, b. Unfortunately, the $-\overline{u'v'}$ profiles do not seem to collapse in any scalings tested. As shown in Fig. 19a, b, $-\overline{u'v'}$ profiles are in reasonably good agreement for the cases of $Re_{\theta,\mathrm{ref}}$=3,400, 13,200, and 20,100, but the $Re_{\theta,\mathrm{ref}}$=7,100 profile is different. The disagreement might be caused by measurement errors although it is doubtful since the near-wall measurements agree (see Fig. 16a, b). On the other hand, the $Re_{\theta,\mathrm{ref}}$=7,100 case has lower freestream velocity than other cases suggesting that the $-\overline{u'v'}$ decay rate in the outer boundary layer may depend on the freestream velocity in a way not captured by the non-dimensional parameters used.

Since $\overline{v'^2}$ and $-\overline{u'v'}$ behave similarly for other non-equilibrium boundary layers examined, the above finding

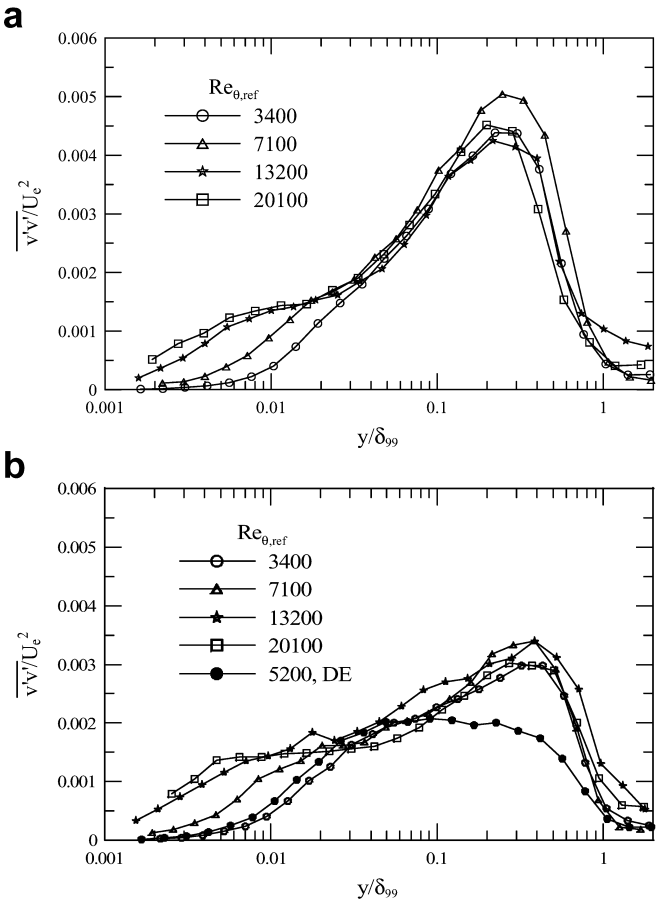

Fig. 18a, b. Reynolds number scaling for $\overline{v'^2}$ for the outer layer in the recovery region. **a** x'=4.00; **b** x'=7.00. *DE* denotes DeGraaff and Eaton (2000)

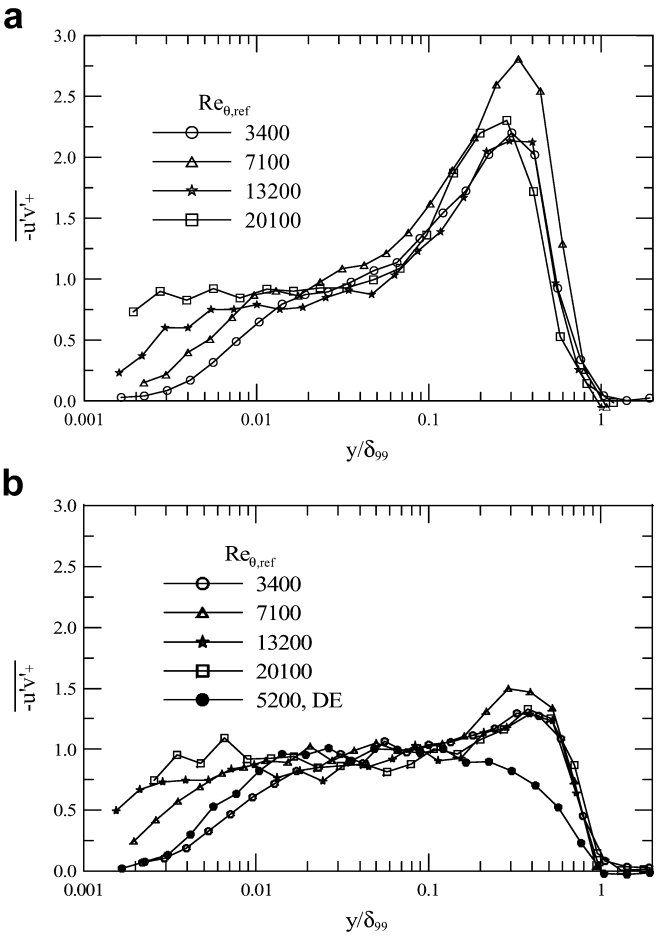

Fig. 19a, b. Reynolds number scaling for $\overline{-u'v'}$ for the outer layer in the recovery region. **a** x'=4.00; **b** x'=7.00. *DE* denotes DeGraaff and Eaton (2000)

is fairly surprising. The wall-normal stress, $\overline{v'^2}$, is expected to continue to decay toward an ordinary boundary layer level, so it will eventually scale on U_τ^2. Overall, it appears that the recovery rates of the three Reynolds stresses toward a flat-plate boundary layer scaling are ordered as follows: $\overline{u'^2}$, $\overline{u'v'}$, and $\overline{v'^2}$ from fastest to slowest.

4 Conclusions

The present study addresses Reynolds number scalings for the mean velocity and Reynolds stresses of a separating, reattaching, and recovering boundary layer for the upstream momentum thickness Reynolds number from 1,100 to 20,100.

A turbulent boundary layer separates on a smoothly contoured ramp, and reattaches a short distance downstream of the ramp trailing edge forming a thin separation bubble. The vortices generated in the separated shear layer dominate the outer layer turbulence in the recovery region. The recovery of the outer layer turbulence is much slower than the mean flow recovery. In contrast, the near-wall turbulence recovers relatively rapidly. As a result, a stress equilibrium layer develops near the wall, although the outer layer turbulence is still energetic and out of equilibrium with the mean flow.

Reynolds number effects on the mean flow are small. For example, the mean separation and reattachment points hardly change except for the lowest Reynolds number case. The velocity deficit law proposed by Zagarola and Smits (1998) holds in most flow regions except for the ramp trailing edge and reattachment regions.

The lowest Reynolds number flow is completely different from the higher Reynolds number flows. The strong Reynolds number effects for this lowest Reynolds number case taken together with earlier work by DeGraaff and Eaton (1999) show conclusively that boundary layers with Re_θ less than 2,000 can not be considered fully turbulent. We believe that modeling information taken at Re_θ less than at least 3,000 should not be considered representative of fully turbulent flows. In model tests of high Reynolds number systems where flow separation may be important, the experiments must insure that Re_θ values greater than 3,000 are maintained. Tripping of a low Reynolds number boundary layer probably is not adequate in order to obtain separation behavior representative of high Reynolds number.

Reynolds number effects on turbulence quantities are large over the full range of Reynolds number. As a consequence, none of the previously known scalings for Reynolds stress works in the separated region. However, Reynolds number similarity for Reynolds stress can be achieved when correct scalings are used. Empirically derived Reynolds number scalings have been found for

different regions of the flow. Inflection point scaling ($y_{\text{in fln}}$ and $U_{\text{in fln}}$) characterizes much of the separated zone and is equivalent to the plane mixing layer scaling in the sense that the scalings represent the height and velocity where Reynolds stresses are maximum. The discovery of the correct Reynolds number scalings is important, especially at reattachment and in the recovery region where CFD faces serious challenges because of the highly non-equilibrium nature of the flow. Turbulence models designed to predict turbulence quantities should be tested to determine if they can capture the observed scaling behavior.

A stress equilibrium layer develops downstream of reattachment regardless of Reynolds number. The law of the wall is accurate in the stress equilibrium layer for the given Reynolds number range. The flat-plate boundary layer scaling for Reynolds stress proposed by DeGraaff and Eaton (2000) is valid within the stress equilibrium layer. The existence of the stress equilibrium layer indicates that the near-wall flow downstream of perturbations recovers independently of the outer layer flow structures.

References

Adams EW, Johnston JP (1988) Flow structure in the near wall zone of a turbulent separated flow. AIAA J 26:932–939

Alving AE, Fernholz HH (1996) Turbulence measurements around a mild separation bubble and downstream of reattachment. J Fluid Mech 322:297–328

Bandyopadhyay PR (1991) Instabilities and large structures in reattaching boundary layers. AIAA J 29:1149–1155

Bandyopadhyay PR, Ahmed A (1993) Turbulent boundary layers subjected to multiple curvatures and pressure gradients. J Fluid Mech 246:503–527

Bradshaw P, Wong FYF (1972) The reattachment and relaxation of a turbulent shear layer. J Fluid Mech 52:113–135

Castillo L, George WK (2001) Similarity analysis for turbulent boundary layer with pressure gradient: outer flow. AIAA J 39: 41–47

Castro IP, Epik E (1998) Boundary layer development after a separated region. J Fluid Mech 374:91–116

Castro IP, Haque A (1987) The structure of a turbulent shear layer bounding a separation region. J Fluid Mech 179:439–468

DeGraaff DB, Eaton JK (1999) Reynolds number scaling of the turbulent boundary layer on a flat plate and on swept and unswept bumps. Technical Report TSD-118, Stanford University

DeGraaff DB, Eaton JK (2000) Reynolds-number scaling of the flat-plate turbulent boundary layer. J Fluid Mech 422:319–346

DeGraaff DB, Eaton JK (2001) A high resolution laser Doppler anemometer: design, qualification, and uncertainty. Exp Fluids 20:522–530

Driver DM, Seegmiller HL, Marvin JG (1987) Time-dependent behavior of a reattaching shear layer. AIAA J 25:914–919

Eaton JK, Johnston JP (1981) A review of research on subsonic turbulent flow reattachment. AIAA J 19:1093–1100

Gillis JC, Johnston JP (1983) Turbulent boundary-layer flow and structure on a convex wall and its redevelopment on a flat wall. J Fluid Mech 135:123–153

Hancock PE (2000) Low Reynolds number two-dimensional separated and reattaching turbulent shear flow. J Fluid Mech 410:101–122

Kim J, Kline SJ, Johnston JP (1980) Investigation of a reattaching turbulent shear layer: flow over a backward-facing step. J Fluids Eng 102:302–308

Littell HS, Eaton JK (1994) Turbulence characteristics of the boundary layer on a rotating disk. J Fluid Mech 266:175–207

Monson DJ, Mateer GG, Menter FR (1993) Boundary-layer transition and global skin friction measurement with an oil-fringe imaging technique. SAE Technical Paper Series No 932550

Ölcmen MS, Simpson RL, George J (2001) Some Reynolds number effects on two- and three-dimensional turbulent boundary layers. Exp Fluids 31:219–228

Perry AE, Schofield WH (1973) Mean velocity and shear stress distributions in turbulent boundary layers. Phys Fluids 16:2068–2074

Pronchick S, Kline S (1983) An experimental investigation of the structure of a turbulent reattaching flow behind a backward facing step. Technical Report MD-42, Stanford University

Samuel AE, Joubert PN (1974) A boundary layer developing in an increasingly adverse pressure gradient. J Fluid Mech 66:481–505

Schofield WH (1981) Equilibrium boundary layers in moderate to strong adverse pressure gradients. J Fluid Mech 113:91–122

Simpson RL, Chew YT, Shivaprasad BG (1981a). The structure of a separating turbulent boundary layer. Part 1. Mean flow and Reynolds stresses. J Fluid Mech 113:23–51

Simpson RL, Chew YT, Shivaprasad BG (1981b) The structure of a separating turbulent boundary layer. Part 2. Higher-order turbulence results. J Fluid Mech 113:53–73

Smits AJ, Wood DH (1985) The response of turbulent boundary layer to sudden perturbations. Ann Rev Fluid Mech 17:321–358

Song S, DeGraaff BD, Eaton JK (2000) Experimental study of a separating, reattaching, redeveloping flow over a smoothly contoured ramp. Int J Heat Fluid Flow 21:512–519

Song S, Eaton JK (2002a) The effects of wall roughness on the separated flow over a smoothly contoured ramp. Exp Fluids 33:38–46

Song S, Eaton JK (2002b) Reynolds number effects on a turbulent boundary layer with separation, reattachment, and recovery. Technical Report TSD-146, Stanford University

Webster DR, DeGraaff DB, Eaton JK (1996) Turbulence characteristics of a boundary layer over a two-dimensional bump. J Fluid Mech 320:53–69

Zagarola MV, Smits AJ (1998) Mean-flow scaling of turbulent pipe flow. J Fluid Mech 373:33–79